Infrared-microwave two-photon spectroscopy: The ν_2 band of NH_3

S. M. Freund* and Takeshi Oka

Herzberg Institute of Astrophysics, National Research Council of Canada, Ottawa, Ontario, K1A OR6, Canada

(Received 2 February 1976)

A spectroscopic method is developed in which the frequency of microwave radiation is added to or subtracted from that of infrared radiation by using two-photon processes in molecules. By utilizing many lines of the CO_2 and N_2O lasers, this method enables us to perform systematic high-resolution spectroscopy in the 10-μm region. Both straightforward two-photon absorption spectroscopy and two-photon Lamb-dip spectroscopy can be used. We describe the theory of this method and its application to the observation of the ν_2 band of $^{14}NH_3$ and $^{15}NH_3$.

I. INTRODUCTION

Two-photon spectroscopy, in which two radiations with very different frequencies are added or subtracted by using the nonlinearity of molecular transition processes, is well known in microwave spectroscopy.[1] With the advent of the laser such experiments have been done by using infrared and microwave radiations.[2] It has been shown that in favorable cases the two-photon processes are sufficiently strong to saturate transitions; thus they have been used for observations of Lamb dips[3] and for pumping molecules in a double-resonance experiment.[4] This technique is particularly useful when combined with molecular gas lasers, because the presence of many laser lines and the tunability of the microwave frequency make this method applicable to systematic high-resolution spectroscopy. In this paper we report our studies on the characteristics of two-photon processes and their application to the infrared spectroscopy of the ν_2 band of NH_3.[5]

II. THEORY

A. Transition probability

The infrared-microwave two-photon processes used in this paper are shown in Fig. 1. A microwave quantum is added to or subtracted from an infrared quantum in the energy-level schemes shown in Figs. 1(a) and 1(b), respectively. The behavior of the molecule is described by the time-dependent Schrödinger equation

$$i\hbar\frac{\partial\Psi}{\partial t}=H\Psi, \tag{1}$$

with

$$H=H_0-\vec{\mu}_p\cdot\vec{E}_m\cos\omega_m t-\vec{\mu}_v\cdot\vec{E}_l\cos\omega_l t,$$

where H_0 is the Hamiltonian of the molecule in free space, μ_p and μ_v are the permanent dipole moment and the vibrational transition dipole moment of the molecule, respectively, and E_m and E_l are the electric field of the microwave (ω_m) and the laser (ω_l) radiation, respectively. Here we are considering radiation fields acting only on near-resonant molecular motions, and neglecting many other interactions. The Schrödinger equation is solved for the case in which

$$\begin{aligned}&\omega_0,\ \omega_l \gg |\omega_0-\omega_l|,\\ &\omega_m,\ \omega_0',\ |\omega_m-\omega_0'| \gg |\omega_0+\omega_0'-\omega_l-\omega_m|,\end{aligned} \tag{2}$$

where $\omega_0\equiv(E_3-E_2)/\hbar$ and $\omega_0'\equiv(E_2-E_1)/\hbar$ are the resonant ir and MW frequencies.

Using the second-order perturbation,[6] we find the transition moment for the two-photon process (in the unit of angular frequency) to be

$$M_2=\langle 1|\vec{\mu}_p\cdot\vec{E}_m|2\rangle\langle 2|\vec{\mu}_v\cdot\vec{E}_l|3\rangle/2\hbar^2(\omega_0-\omega_l). \tag{3}$$

When this expression is compared with the transition moment for the normal single-photon process,

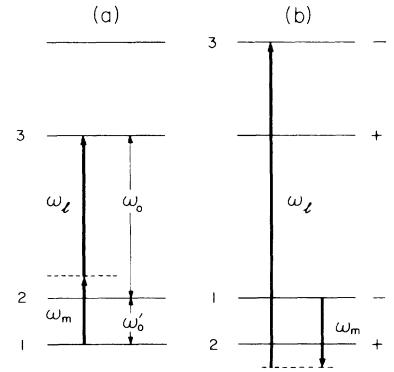

FIG. 1. Energy-level schemes for ir-MW two-photon processes. The microwave radiation (ω_m) is (a) added to or (b) subtracted from the infrared laser radiation (ω_l). The "+" and "−" signs beside levels indicate parity relation of the inversion-rotation-vibration levels of NH_3.

$$M_1 = \langle 2 | \vec{\mu}_v \cdot \vec{E}_l | 3 \rangle / \hbar, \tag{4}$$

we find that the transition probability of the two-photon process is smaller than the corresponding single-photon process by a factor

$$\left|\frac{M_2}{M_1}\right|^2 = \left|\frac{\langle 1 | \vec{\mu}_p \cdot \vec{E}_m | 2 \rangle}{2\hbar(\omega_0 - \omega_l)}\right|^2 \equiv \left|\frac{x_m}{\omega_0 - \omega_l}\right|^2, \tag{5}$$

where x_m is defined as $\langle 1 | \vec{\mu}_p \cdot \vec{E}_m | 2 \rangle / 2\hbar$. By using the microwave power density of 0.5–2 W/cm^2 ($E = 25$–50 V/cm), $\mu_p = 1.468$ D,[7] and the direction cosine of $\frac{1}{2}$–1, we find that the typical value of $x_m/2\pi$ is 5–15 MHz. Since the absorption coefficients of infrared spectral lines are typically 1 cm^{-1} in the pressure-broadened region, we can reach $\Delta\nu \sim 10$ GHz if the sensitivity of the infrared detection is 10^{-6} cm^{-1}. Using a 1-m cell, this corresponds to detection of the absorption of 10^{-4}, which is easily achieved. By using somewhat higher sensitivity of detection and using the CO_2 and N_2O laser lines which have line spacings of 0.5–2 cm^{-1}, we can perform systematic spectroscopy over the entire range of laser oscillation.

B. Line shape and saturation

If we expand the wave function in Eq. (1) into a linear combination of the stationary-state wave functions $\psi_k^{(0)}$,

$$\Psi = a_1(t)\Psi_1^{(0)} + a_2(t)\Psi_2^{(0)} + a_3(t)\Psi_3^{(0)}, \tag{6}$$

we obtain, after applying the standard procedure of the rotating-wave approximation, equations of motion for the coefficients as (see, for example, Refs. 8 and 9)

$$\begin{aligned}
\dot{\alpha}_1(t) &= -iM_2 \exp[-i(\omega_0 + \omega_0' - \omega_l - \omega_m + \delta + \delta_m)t]\tfrac{1}{2}\alpha_3(t), \\
\dot{\alpha}_2(t) &= 0, \\
\dot{\alpha}_3(t) &= -iM_2^* \exp[i(\omega_0 + \omega_0' - \omega_l - \omega_m + \delta + \delta_m)t]\tfrac{1}{2}\alpha_1(t),
\end{aligned} \tag{7}$$

where

$$\delta = |\langle 2 | \vec{\mu}_v \cdot \vec{E}_l | 3 \rangle|^2 / (\omega_0 - \omega_l) \tag{8}$$

and

$$\delta_m = |\langle 1 | \vec{\mu}_p \cdot \vec{E}_m | 2 \rangle|^2 [1/(\omega_0' - \omega_m) + 1/(\omega_0' + \omega_m)]$$

are high-frequency Stark shifts and $\alpha_k(t)$ and $a_k(t)$ are related by phase factors $\alpha_k(t) = e^{i\epsilon_k} a_k(t)$, with $\epsilon_1 = -\delta_m$, $\epsilon_2 = \delta_m - \delta$, and $\epsilon_3 = \delta$. Since $\langle 1 | \vec{\mu}_p \cdot \vec{E}_m | 2 \rangle / h$ is of the order of 15 MHz, $\delta_m/2\pi$ is less than 1 MHz if $|\omega_0' - \omega_m|/2\pi > 300$ MHz and is neglected in the following treatment; since $\mu_v = 0.23$ D (Ref. 11) and $E_l \sim 200$ V/cm, δ is of the same order of magnitude and is also neglected.

A comparison of the equations of motion given in Eq. (7) with those for a normal single-photon process (see, for example, Sec. 40 of Ref. 10) indicates that we can treat line shape and efficiency of saturation of the two-photon processes similarly to those of single-photon processes. Therefore the absorption coefficient of two-photon processes monitored by infrared radiation is given by the Voigt profile[12]

$$\alpha = \frac{2h\nu\gamma}{3c}\left|\frac{M_2}{E_l}\right|^2 \times \int_{-\infty}^{+\infty} \frac{N(v)\,dv}{[\omega_0 + \omega_0' - (\omega_l + \omega_m)(1 + v/c)]^2 + \gamma^2 + M_2^2}, \tag{9}$$

where $N(v)$ is the Maxwellian velocity distribution, which is expressed in terms of the number of molecules per cubic centimeter, N, and the average velocity along the Z axis, v_0, as

$$N(v) = Ne^{-(v/v_0)^2}/\sqrt{\pi}\,v_0, \tag{10}$$

and γ is the pressure broadening of the two-photon spectral line. For NH_3 at room temperature, the average Doppler width $kv = (2kT/m)^{1/2}(2\pi/\lambda)$ is calculated to be about $2\pi \times 40$ MHz at 10 μm.

The pumping efficiency Φ is estimated to be[13]

$$\Phi = \frac{n_1^0(v) - n_3^0(v) - n_1(v) + n_3(v)}{n_1^0(v) - n_3^0(v)} = \frac{M_2^2}{[\omega_0 + \omega_0' - (\omega_l + \omega_m)(1 + v/c)]^2 + \gamma^2 + M_2^2}, \tag{11}$$

where $n_1(v)$ and $n_3(v)$ are the molecular population of levels 1 and 3 and $n_1^0(v)$ and $n_3^0(v)$ are their equilibrium values. Equation (11) shows that we can saturate the two-photon transition for molecules with certain velocity if $M_2 \gtrsim \gamma$, that is, for a pressure of

$$P \lesssim \frac{\langle 1 | \vec{\mu}_p \cdot \vec{E}_m | 2 \rangle \langle 2 | \vec{\mu}_v \cdot \vec{E}_l | 3 \rangle}{2\hbar^2 |\nu_0 - \nu_l| (\Delta\nu)_p}, \tag{12}$$

where $(\Delta\nu)_p$ is the pressure-broadening parameter. By using $\langle 1 | \vec{\mu}_p \cdot \vec{E}_m | 2 \rangle / 2h \sim 10$ MHz, $\mu_v = 0.23$ D,[11] $E_l \sim 200$ V/cm (power density ~ 30 W/cm^2), direction cosine of 1–$\frac{1}{2}$, and the pressure-broadening parameter of 24 MHz/Torr,[14] we find we can saturate the two-photon transition with $\Delta\nu = 1$ GHz up to the pressure of 10 mTorr, or that with $\Delta\nu = 10$ GHz up to the pressure of 1 mTorr. Thus two-photon Lamb-dip spectroscopy[3] or two-photon saturation[4] is feasible.

C. Two-photon Lamb dips

A theory of two-photon Lamb dips has been developed by Shimizu by using the density-matrix formalism.[15] We will describe his results with slight modifications. We consider the situation shown in Fig. 2; the molecule with an axial velocity v experiences the radiation field

$$E = \tfrac{1}{2}(E_+ e^{-i(\omega_l + k_v)t} + E_- e^{-i(\omega_l - k_v)t} + E_m e^{-i\omega_m t} + \text{c.c.}). \tag{13}$$

The Doppler shift for the microwave radiation is neglected in Eq. (13). The response of an ensemble of the molecules with the energy-level system shown in Fig. 1(a) is obtained by solving the density-matrix equation

$$\frac{d\rho'}{dt} = -\frac{i}{\hbar}[H, \rho'] - \Gamma(\rho' - \rho'^{(0)}), \tag{14}$$

with the Hamiltonian

$$H = \begin{bmatrix} W_3 & -\mu_{23}E & 0 \\ -\mu_{23}E & W_2 & -\mu_{12}E \\ 0 & -\mu_{12}E & W_1 \end{bmatrix}, \tag{15}$$

and the damping coefficient Γ is assumed to be γ_0 $(=1/T_1)$ and γ $(=1/T_2)$ for all diagonal and nondiagonal elements, respectively, of the density matrix. This assumption does not introduce serious error, since (1) the spontaneous emission time for the infrared is much longer than the collision time and (2) pressure-broadening parameters do not depend critically on the vibration-rotation state. The equations of motion for the components of the density matrix are given by the standard procedure as

$$\begin{aligned}
&\dot\rho_0 + \gamma_0(\rho_0 - \rho_0^{(0)}) = i(-2\mu_{23}E\rho'_{32} + \mu_{12}E\rho'_{21})/\hbar + \text{c.c.},\\
&\dot\rho_m + \gamma_0(\rho_m - \rho_m^{(0)}) = i(\mu_{23}E\rho'_{32} - 2\mu_{12}E\rho'_{21})/\hbar + \text{c.c.},\\
&\dot\rho'_{32} + (i\omega_0 + \gamma)\rho'_{32} = -i(\mu_{23}E\rho_0 + \mu_{12}E\rho'_{31})/\hbar,\\
&\dot\rho'_{31} + [i(\omega_0 + \omega'_0) + \gamma]\rho'_{31} = i(\mu_{23}E\rho'_{21} - \mu_{12}E\rho'_{32})/\hbar,\\
&\dot\rho'_{21} + (i\omega'_0 + \gamma)\rho'_{21} = i(\mu_{23}E\rho'_{31} - \mu_{12}E\rho_m)/\hbar,
\end{aligned} \tag{16}$$

where notations $\rho_0 \equiv \rho'_{33} - \rho'_{22}$ and $\rho_m \equiv \rho'_{22} - \rho'_{11}$ have been used. We then substitute the field given in Eq. (3) and use the rotating-wave approximation, that is, we substitute for the off-diagonal elements $\rho'_{21} = \rho_{21}e^{-i\omega'_0 t}$, $\rho'_{32} = \rho_{32}e^{-i\omega_0 t}$, and $\rho'_{31} = \rho_{31}e^{-i(\omega_0 + \omega'_0)t}$ and retain terms which oscillate with frequencies $\omega_l - \omega_0 \equiv \Omega$ and $\omega_m - \omega'_0 \equiv \delta$. This is based on the order-of-magnitude scheme given in Eq. (2); the terms with $\omega_m + \omega'_0$ are dropped since these terms do not appear in two-photon formula discussed in Sec. II A.

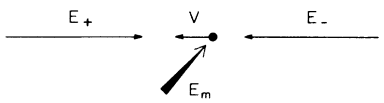

FIG. 2. Basic situation considered in the discussion of two-photon Lamb dips. The molecule with a velocity component v along the direction of propagation of the laser radiation interacts with the laser radiation field E_+ and E_- and with the microwave radiation field E_m, which have frequencies $\omega_l(1 + v/c)$, $\omega_l(1 - v/c)$, and ω_m, respectively.

We obtain the following equations:

$$\begin{aligned}
&\dot\rho_0 + \gamma_0(\rho_0 - \rho_0^{(0)}) = -y_m^*\rho_{21} + 2y_0^*\rho_{32} + \text{c.c.},\\
&\dot\rho_m + \gamma_0(\rho_m - \rho_m^{(0)}) = 2y_m^*\rho_{21} - y_0^*\rho_{32} + \text{c.c.},\\
&\dot\rho_{32} + \gamma\rho_{32} = y_m^*\rho_{31} - y_0\rho_0,\\
&\dot\rho_{31} + \gamma\rho_{31} = -y_m\rho_{32} + y_0\rho_{21},\\
&\dot\rho_{21} + \gamma\rho_{21} = -y_m\rho_m - y_0^*\rho_{31},
\end{aligned} \tag{17}$$

where notations

$$\begin{aligned}
&y_0 = i(x_+e^{-i\Omega_+ t} + x_-e^{-i\Omega_- t}), \quad y_m = ix_m e^{-i\delta t},\\
&x_\pm = \mu_{23}E_\pm/2\hbar, \quad x_m = \mu_{12}E_m/2\hbar, \quad \Omega_\pm = \Omega \pm u,\\
&u = kv
\end{aligned}$$

have been introduced.

Equations (17) are solved by using the standard perturbation method in which the density matrix ρ is expanded as

$$\rho = \rho^{(0)} + \rho^{(1)} + \rho^{(2)} + \cdots. \tag{18}$$

Equations (17) can then be formally integrated with respect to time to give

$$\rho_0^{(n)} = e^{-\gamma_0 t}\int_{-\infty}^{t}(-y_m^*\rho_{21}^{(n-1)} + 2y_0^*\rho_{32}^{(n-1)})e^{\gamma_0 t}\,dt + \text{c.c.}, \tag{19}$$

etc. We set the "initial condition" to be $\rho_0^{(0)} = -1$, $\rho_m^{(0)} = 0$, and $\rho_{32}^{(0)} = \rho_{31}^{(0)} = \rho_{21}^{(0)} = 0$ and calculate $\rho^{(n)}$ by iteration. The explicit forms of y_m and y_0 given after Eqs. (17) indicate that these operators "add" time dependence $e^{-\delta t}$ and $e^{-\Omega_\pm t}$, respectively, to $\rho^{(n-1)}$, and their complex conjugate y_m^* and y_0^* add $e^{\delta t}$ and $e^{\Omega_\pm t}$; thus we can consider them as annihilation and creation operators. An examination of the structure of Eqs. (17) shows that y_0 and y_0^*, and y_m and y_m^*, appear alternatively in the iteration. Therefore a component of $\rho^{(n)}$ is expressed in general as an n product of the factors of the form

$$\frac{\pm ix}{i(-j\Omega + lu - m\delta) + \gamma}, \tag{20}$$

where the integers $j = 1$ or 0, $m = 1$ or 0, and $|l| \leq n$. The components of $\rho^{(n)}$ thus calculated describe the response of an ensemble of molecules under the radiation fields.

Since the experiment is conducted by monitoring the laser radiation, we are interested in the molecular susceptibility with respect to the laser radiation, that is, the polarization $\mu_{23}\rho_{32}N(u)du$ divided by the field $E_+e^{-i\Omega_+ t}$. When integrated over the velocity this gives the nth-order susceptibility

$$\chi^{(n)} = \mu_{23} \int_{-\infty}^{+\infty} N(u) \rho_{32}^{(n)} (E_+ e^{-i\Omega_+ t})^{-1} \, du, \qquad (21)$$

where $N(u)$ is the Maxwellian velocity distribution defined in Eq. (10) (we now express the velocity in terms of the Doppler shift $u = kv$). Equation (21) shows that in order to calculate $\chi^{(n)}$, which is independent of time, we have to use $\rho_{32}^{(n)}$ with the time dependence of $e^{-i\Omega_+ t}$, i.e., $\rho_{32}^{(n)}$ for which the last factor given by (20) has $j=1$ and $l=-1$. $\chi^{(n)}$ is also contributed from $\rho_{23}^{(n)}$ but inclusion of this term together with $E_+^* e^{i\Omega_+ t}$ gives the same susceptibility as given in Eq. (21).

Just as in ordinary Lamb dips, the dips are caused by molecules with $u=0$. Since in our experimental conditions, γ_0 and γ are much smaller than the Doppler width u_0, we can approximate $\chi^{(n)}$ in Eq. (21) by taking $N(0)$ out of the integral. The remaining integration can then be performed by using the method of contour integration by summing up residues of poles for the n product of the expression given in (20). The terms with all poles on one side of the real axis only (that is, if all l's are positive or all l's are negative) vanish after the contour integration. As mentioned by Shimizu, recognition of this fact simplifies the iteration procedure considerably.

For the normal single-photon Lamb dip [we set $y_m = 0$ in Eqs. (17)], the relevant density-matrix element appears at the third-order iteration as

$$\rho_{32}^{(3)} = -\left(\frac{-i x_-}{-i\Omega_- + \gamma}\right)\left(\frac{-2i x_-^*}{\gamma_0}\right)\left(\frac{-i x_+}{-i\Omega_+ + \gamma}\right) e^{-i\Omega_+ t}, \qquad (22)$$

and the susceptibility is calculated to be

$$\chi^{(3)} = \frac{\pi \mu_{23}^2 |x_-|^2 N(0)}{\hbar \gamma_0} \frac{1}{\omega_l - \omega_0 + i\gamma}. \qquad (23)$$

The iteration procedure for $\chi^{(3)}$ is expressed diagrammatically as

$$\begin{array}{cccccccc} \rho_0^{(0)} & \rightarrow & \rho_{32}^{(1)} & \rightarrow & \rho_0^{(2)} & \rightarrow & \rho_{32}^{(3)}, \\ 0 & & -\Omega_- & & 0 & & -\Omega_+ \end{array} \qquad (24)$$

where the expression under ρ indicates the frequency of ρ. Since we use perturbation treatment, Eq. (23) applies to the case where saturation is small.

The susceptibility for the two-photon Lamb dip is derived from a fifth-order term $\rho_{32}^{(5)}$, which is obtained after an iteration procedure,

$$\begin{array}{ccccccccccc} \rho_0^{(0)} & \rightarrow & \rho_{32}^{(1)} & \rightarrow & \rho_{31}^{(2)} & \rightarrow & \rho_{21}^{(3)} & \rightarrow & \rho_{31}^{(4)} & \rightarrow & \rho_{32}^{(5)}, \\ 0 & & -\Omega_- & & -\Omega_- - \delta & & -\delta & & -\Omega_+ - \delta & & -\Omega_+ \end{array} \qquad (25)$$

as

$$\rho_{32}^{(5)} = -\frac{-i x_-}{-i\Omega_- + \gamma} \frac{-i x_m}{-i(\Omega_- + \delta) + \gamma} \frac{i x_-^*}{-i\delta + \gamma} \times \frac{i x_+}{-i(\Omega_+ + \delta) + \gamma} \frac{-i x_m^*}{-i\Omega_+ + \gamma} e^{-i\Omega_+ t}. \qquad (26)$$

This expression has poles above the real axis of $u = \Omega + i\gamma$ and $\Omega + \delta + i\gamma$. Since we are considering the case $\Omega \gg u_0$ in this section, the former pole does not contribute to susceptibility [$N(\Omega) \ll 1$]. After the integration and using approximations $\Omega + \delta \sim 0$ and $\Omega \gg \gamma$, we find

$$\chi^{(5)} = -\frac{\pi \mu_{23}^2 |x_-|^2 |x_m|^2 N(0)}{2\hbar (\omega_l - \omega_0)^3} \frac{i}{(\omega_l + \omega_m - \omega_0 - \omega_0') + i\gamma}, \qquad (27)$$

which gives a sharp resonance at $\omega_l + \omega_m = \omega_0 + \omega_0'$. Another contribution to two-photon Lamb dips results in a seventh-order term $\rho_{32}^{(7)}$, which is obtained after an iteration procedure,

$$\begin{array}{ccccccccccccccc} \rho_0^{(0)} & \rightarrow & \rho_{32}^{(1)} & \rightarrow & \rho_{31}^{(2)} & \rightarrow & \rho_{32}^{(3)} & \rightarrow & \rho_0^{(4)} & \rightarrow & \rho_{32}^{(5)} & \rightarrow & \rho_{31}^{(6)} & \rightarrow & \rho_{32}^{(7)}, \\ 0 & & -\Omega_- & & -\Omega_- - \delta & & -\Omega_- & & 0 & & -\Omega_+ & & -\Omega_+ - \delta & & -\Omega_+ \end{array} \qquad (28)$$

which gives

$$\rho_{32}^{(7)} = -\frac{-i x_-}{-i\Omega_- + \gamma} \frac{-i x_m}{-i(\Omega_- + \delta) + \gamma} \frac{-i x_m^*}{-i\Omega_- + \gamma} \frac{-2i x_-^*}{\gamma_0} \frac{-i x_+}{-i\Omega_+ + \gamma} \frac{-i x_m}{-i(\Omega_+ + \delta) + \gamma} \frac{-i x_m^*}{-i\Omega_+ + \delta} e^{-i\Omega_+ t}. \qquad (29)$$

The susceptibility near $\Omega + \delta = 0$ is given as

$$\chi^{(7)} = \frac{\pi \mu_{23}^2 |x_-|^2 |x_m|^4 N(0)}{\hbar \gamma_0 |\omega_l - \omega_0|^4} \frac{1}{(\omega_l + \omega_m - \omega_0 - \omega_0') + i\gamma}. \qquad (30)$$

D. Line shape of the Lamb dip

A comparison of Eqs. (23), (27), and (30) indicates that $\chi^{(3)}$ and $\chi^{(7)}$ have similar line shapes but the shape of $\chi^{(5)}$ is different. The extra factor of i in the numerator of $\chi^{(5)}$ makes the imaginary (absorption) part of $\chi^{(5)}$ be of dispersion shape and the real (dispersion) part of $\chi^{(5)}$ be of the normal Lorentzian absorption shape. Therefore, if the observation is made through absorption, $\chi^{(5)}$ gives a dispersion-shaped Lamb dip; if the observation is made through dispersion, $\chi^{(5)}$ gives a Lorentzian absorption shape. Experimentally we can observe both cases by using different frequency settings of the laser, as will be discussed in Sec. II E. For spectroscopic purposes, we set the frequency of the laser at the center of the gain profile and observe absorption; then $\chi^{(5)}$ gives dips with a dispersion shape.

This behavior of $\chi^{(5)}$ is due to the fact that in the process given in Eq. (25), contrary to the normal process given in Eq. (24), the population ρ_0 does not appear except at the beginning. The "saturation" is not really done. We do not yet know how to interpret this process physically. The seventh-order process given in Eq. (28) is easier to interpret. The saturation by the two-photon process is complete at $\rho_0^{(4)}$ and the hole burned by a two-photon process using E_+ is monitored by the same two-photon process using E_-. $\chi^{(7)}$ gives the same form as the normal Lamb dip. The ratio of $\chi^{(5)}$ to $\chi^{(7)}$ is found to be

$$|\chi^{(5)}/\chi^{(7)}| = \gamma_0 |\omega_l - \omega_0| / |x_m|^2 . \tag{31}$$

This formula indicates that for a large value of $|\omega_l - \omega_0|$ ($|\omega_l - \omega_0| \gg |x_m|^2\gamma_0 \sim 1000$ MHz), the contribution of $\chi^{(5)}$ dominates and the two-photon Lamb dips observed with the laser set at the center of the gain profile show dispersion shapes. For smaller $\omega_l - \omega_0$, however, the shape varies between the dispersion and the Lorentzian absorption shape depending on the rf field ($\sim x_m$) and the pressure ($\sim\gamma_0$).

E. Intracavity arrangement

In the experimental arrangement used for our observation of two-photon Lamb dips, the absorbing gas was placed inside the laser cavity and the output power of the laser was monitored. Therefore the sharp variation of the bulk susceptibility of the gas at the two-photon resonance condition, which was calculated in Sec. II D, is added as a perturbation to the susceptibility of the laser gain medium. The resulting sharp variation of the laser output power is monitored. We can qualitatively analyze this situation by using the self-consistency equations of Lamb,[16,17]

$$\dot{E} + \nu E/2Q = -\tfrac{1}{2}\nu E \,\mathrm{Im}(\chi), \quad \nu + \dot{\phi} = \Omega - \tfrac{1}{2}\nu \,\mathrm{Re}(\chi), \tag{32}$$

where E is the electric field of the laser radiation, ϕ is its phase, Q is the quality factor of the cavity, and ν and Ω are the angular resonance frequencies of the gain medium and laser cavity, respectively. Equation (32) indicate that the imaginary part of χ changes the laser field and the real part of χ the laser frequency. Both of these changes affect the laser output power, but the importance of the two changes depends on the setting of the laser frequency.

If the laser frequency is set at the center of the laser gain profile, the intensity of the laser radiation I does not vary much with a small variation in frequency ($\partial I/\partial\omega \sim 0$). In this case two-photon Lamb dips are observed through the imaginary part of χ. For the purpose of spectroscopy this arrangement was used. If the laser frequency is set off-center on the gain profile, the intensity of the laser radiation is very dependent on the frequency and the contribution of the real part of χ becomes dominant. Since the sign of the derivative $\partial I/\partial\omega$ varies depending on whether the cavity frequency is set higher than the frequency of the gain molecule or lower, we can discriminate the dispersion effect of observing the change of phase of the dips depending on the laser-cavity tuning.

III. TWO-PHOTON SPECTROSCOPY OF NH_3

A. Experimental setup

The observation of the straightforward ir-MW two-photon spectrum was done by using waveguide cells outside the laser cavity. A block diagram of the apparatus is given in Fig. 3. The CO_2- or N_2O-gas laser consisted of a water-cooled 1.8-m gain cell with a concave mirror of 5 m radius at one end, and a plane grating blazed at 10 μm at the other. The laser was tuned to the

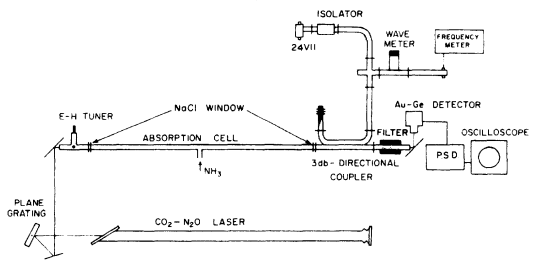

FIG. 3. Block diagram of the apparatus used for straightforward ir-MW two-photon spectroscopy.

individual CO_2 or N_2O line by adjusting the angle of the grating. The power was taken from the zeroth-order reflection of the grating, passed through the sample cell, and detected by a Au-Ge detector. The two-photon absorption cell was made from K-band waveguides of varying length (1–4 m). It was sealed by two 1-mm-thick NaCl windows and an NH_3 sample with a pressure of 50 mTorr to 3 Torr was used. At the initial stage of the experiment a high-power (20 W) klystron (Elliott 12TFK2) was used with amplitude modulation as a microwave source.[2] This enabled us to observe the two-photon absorption by video detection. However, in subsequent experiments, less powerful OKI klystrons (24V11, 30V12, and 35V11) which generate 0.5–1.5 W of power were used with frequency modulation (~ 20 KHz), because of their wider frequency coverage. The microwave power was coupled into the waveguide cell through a 3-dB directional coupler. The E-H tuner at the end of the waveguide helped the microwave matching. A cutoff filter was placed at the ir-detector end of the cell, because we found that the Au-Ge detector was also sensitive to the microwave power. In principle we could detect a two-photon absorption by detecting either of the two radiations, but because of more energy per photon, detecting the infrared radiation was more efficient. The signal was processed through a phase-sensitive detector and displayed on an oscilloscope.

B. Observed spectrum

The observed two-photon spectrum of NH_3 was in accordance with the theoretical shape given in Eq. (9). The absorption has a Doppler half-width of about 35 MHz, as calculated from $\Delta\nu_0 = \nu(2kT\ln 2/M)^{1/2}/c$. The intensity is proportional to the applied microwave power and is inversely proportional to the square of the frequency discrepancy $(\omega_0 - \omega_l)$, as expected from the factor in Eq. (9) of

$$\left|\frac{M_2}{E_l}\right|^2 = \left|\frac{\langle 1|\vec{\mu}_p\cdot\vec{E}_m|2\rangle\langle 2|\vec{\mu}_v\cdot\vec{E}_l|3\rangle}{2\hbar^2(\omega_0-\omega_l)E_l}\right|^2. \quad (33)$$

Two-photon transitions with small $|\omega_0 - \omega_l|$ could be observed by video detection.[2] However, for all but a few transitions frequency modulation and phase-sensitive detection were used.

Since the microwave transitions of NH_3 used in this paper are all between inversion levels ($\Delta J = 0$, $\Delta K = 0$), the dependence of the microwave matrix element on the rotational quantum numbers is[7]

$$\langle 1|\vec{\mu}_p\cdot\vec{E}_m|2\rangle = [KM/J(J+1)]\mu_p E_m. \quad (34)$$

Therefore transitions with larger K values showed stronger signals. No two-photon transition was observed for levels with $K = 0$ for which one level of the inversion doublet is missing because of the Pauli principle. From an examination of the M dependence of the transition moments for $\Delta J = 0$ and $\Delta J = \pm 1$ transitions, we find that an experimental configuration with $\vec{E}_l \| \vec{E}_m$ is preferable for the $\Delta J = 0$ transitions and that with $\vec{E}_l \perp \vec{E}_m$ is preferable for the $\Delta J = \pm 1$ transitions. However, this was not as critical as in the case of two-photon transitions between degenerate levels, where a destructive interference makes the transition probability extremely small for unfavorable experimental conditions.[18,9] Most of the two-photon observation in the present paper was done with a configuration $\vec{E}_l \| \vec{E}_m$.

A complication was introduced by the resonant characteristics of the microwave circuit. The effect of microwave mismatch was more serious in two-photon spectroscopy than that for straight microwave spectroscopy because (a) the intensity of the two-photon absorption is a sensitive function of the microwave power, and (b) the linewidth of the two-photon spectrum is comparable to that of microwave mismatch. The effect of microwave mismatch often caused several sharp features separated by the frequency $c/2L$, which ranged from 150 to 38 MHz for the waveguide length $L = 1$–4 m. We have not tried to remove this resonance, because it increased microwave field in the cell and also helped us to search for two-photon transitions.

In the search for the lines, the result of the laser Stark spectroscopy by Schimizu[19] was of great help. Two-photon spectroscopy has one advantage over Stark spectroscopy in that it can be applied equally to cases with positive and negative $\omega_0 - \omega_l$; the Stark shift with nondegenerate levels often moves only to one direction until the "forbidden" transitions acquire sufficient intensities.

Two examples of observed two-photon absorption are given in Fig. 4. Figure 4(a) shows the two-photon $sQ(4,4)$ transition of $^{14}NH_3$ observed by using the $P(11)$ line of the N_2O laser. [In this paper we use the notation given by Garing, Nielsen, and Rao[20] in specifying the vibration-rotation energy levels. Thus s and a specify two-photon transitions between lower (symmetric) inversion levels and upper (antisymmetric) inversion levels, respectively; they correspond to Figs. 1(a) and 1(b), respectively.] P, Q, and R correspond to $\Delta J = -1$, 0, and 1, respectively, and the numbers in parentheses show values of J and K of the ground state. Since ΔK is always 0 for the ν_2 band, the information about the change of K is

omitted. For the $sQ(4,4)$ transition, $\Delta\nu = \nu_0 - \nu_l$ is 12.3 GHz. The fact that we can observe transitions with such large $\Delta\nu$ using a short time constant of detection (30 msec) demonstrates the sensitivity of this method. The linewidth shown in Fig. 4(a) is much narrower than the Doppler width or the pressure-broadening width; this narrow line is caused by mismatch and resonance in the microwave circuit. Although this helps us to find the transition, the accuracy of frequency measurement is reduced. The derivative shape of the line is due to the frequency modulation and phase-sensitive detection.

Figure 4(b) shows the two-photon $sQ(4,4)$ transition of $^{15}NH_3$ observed by using the $P(15)$ line of the N_2O laser. Here we used a low pressure (0.3 Torr) and a low amplitude of frequency modulation to demonstrate the effect of microwave resonance convoluted by the broad Doppler profile of the line. The cell length was 4 m and the spacing of the sharp features corresponds to $c/2L$. In locating the line center, we measured the center of each feature and took a weighted mean of the frequencies.

Observed two-photon spectral lines are given in Table I. Practically all Q-branch lines with $K \gtrsim \frac{1}{2}J$ have been observed in the region where CO_2 or N_2O laser lines are available. The maximum value of $\Delta\nu$ observed was 12.3 GHz for the line shown in Fig. 4(a). This limit arose because of availability of the pumping klystron rather than the sensitivity of the apparatus. We believe it is possible to observe two-photon transitions with $\Delta\nu$ of 1 cm^{-1} without much difficulty. The uncertainty of the line positions is caused by (a) the large linewidth, (b) the distortion of signals by microwave resonance, and (c) uncertainty in centering the laser line. We feel that problem (b) causes the largest error, and we estimate the accuracy of frequency to be ±30 MHz.

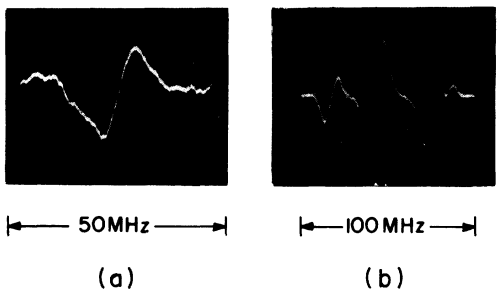

FIG. 4. Examples of ir-MW two-photon absorption signals. (a) The $sQ(4,4)$ two-photon transition of $^{14}NH_3$ observed by using the N_2O $P(11)$ line ($\nu_m = 36.46$, $\Delta\nu = 12.32$ GHz). Sample pressure was 2 Torr and the time constant of detection was 30 msec. (b) The $sQ(4,4)$ two-photon transition of $^{15}NH_3$ observed by using the N_2O $P(15)$ line ($\nu_m = 23358$, $\Delta\nu = 312$ MHz). Sample pressure was 0.3 Torr. The structure of the line is caused by microwave mismatch.

IV. TWO-PHOTON LAMB-DIP SPECTROSCOPY OF NH_3

A. Experimental setup

The observation of the ir-MW two-photon Lamb-dip spectrum was accomplished by using a waveguide cell containing NH_3 at low pressure which was placed *inside* the laser cavity. A block diagram of the apparatus is given in Fig. 5. The CO_2-N_2O laser consisted of a water-cooled 2.5-m gain cell with a concave mirror of 5 m radius at one end and a plane grating blazed for 10 μm at the other end. The assembly which included the intracavity cell was mounted on an Invar frame to make a cavity of 3.8 m length. The wavelength selection was done by rotating the plane grating and the output power was taken from the zeroth-order reflection of the grating. The concave mirror was mounted on a piezoelectric translator and the frequency of the laser was stabilized at the maximum of the gain profile by using a Lansing stabilizer circuit.

The two-photon Lamb-dip cell, which was 80 cm long, was constructed by using a commercial "magic T" and two waveguide extensions (RG-910, 16 × 8mm) sealed with NaCl windows at the Brewster angle. The cell was placed in the laser cavity near the grating, such that the microwave electric field was parallel to the laser electric field. Microwave radiation of about 1 W, generated by an OKI 24V11 klystron (klystron 1 in Fig. 5) was introduced into the cell through the E arm of the "magic T." The microwave frequency was modulated and swept by applying a 20-kHz square-wave voltage and a low-frequency sawtooth voltage to the reflector of the klystron. Klystron 2 in Fig. 5 is a second OKI 24V11 klystron which was used for the observation of coherence splitting described in Sec. II C. The two-photon Lamb dip was detected as a sharp variation of the laser output power by using a Pb-Sn-Te detector. The signal was displayed on an oscilloscope after processing by a phase-sensitive detector. The frequency of the K-band microwave radiation was measured by beating it with the second or third harmonic of X-band radiation generated by the Varian X-13 klystron.

B. Observed Lamb dips

Some examples of the observed two-photon Lamb dips are shown in Fig. 6. Figure 6(a) shows the two-photon transition $aQ(1,1)$ observed by using

TABLE I. Two-photon spectral lines of $^{14}NH_3$.

Two-photon transition	Laser line [a]	ν_m [b] (GHz)	$\Delta\nu$ [b] (GHz)	Pressure (Torr)
$aQ(1,1)$	N_2O $R(37)$	23.991	− 0.297	0.05
$sR(1,1)$	CO_2 $R(14)$	22.290	1.404	0.9
$sQ(2,2)$	N_2O $P(9)$	27.097	3.374	0.6
$sQ(2,2)$	CO_2 $P(34)$	33.674	9.951	2
$aQ(2,2)$	CO_2 $R(8)$	22.797	0.926	0.05
$sR(2,2)$	CO_2 $R(48)$	27.488	3.765	1
$sQ(2,1)$	N_2O $P(8)$	24.725	1.626	0.1
$sQ(3,3)$	N_2O $P(10)$	35.841	11.971	2.1
$aQ(3,3)$	CO_2 $R(8)$	34.677	−10.807	0.5
$aQ(3,3)$	N_2O $R(36)$	22.654	1.216	0.05
$aQ(3,3)\Delta K=3$	N_2O $R(36)$	25.523	− 1.653	0.5
$aQ(3,2)$	CO_2 $R(8)$	31.826	− 8.992	1
$sQ(3,2)$	N_2O $P(8)$	23.181	0.347	0.1
$sQ(4,4)$	N_2O $P(11)$	36.439	12.300	2.2
$sQ(4,2)$	CO_2 $P(32)$	25.173	3.470	0.2
$sQ(5,5)$	N_2O $P(12)$	28.647	4.141	0.7
$aQ(5,5)$	CO_2 $R(6)$	27.523	− 2.990	0.05
$sQ(5,4)$	CO_2 $P(34)$	27.956	5.303	2.5
$aQ(5,4)$	CO_2 $R(6)$	22.109	0.544	0.05
$sQ(5,3)$	CO_2 $P(32)$	22.248	0.963	0.4
$sQ(5,3)$	N_2O $P(7)$	22.818	1.533	0.4
$aQ(5,3)$	N_2O $R(35)$	27.859	− 6.574	1.5
$aR(5,2)$	CO_2 $R(30)$*	21.180	− 0.809	0.1
$sQ(6,6)$	CO_2 $P(38)$	34.501	9.445	3
$sQ(6,5)$	N_2O $P(10)$	21.252	− 1.480	0.5
$aQ(6,4)$	N_2O $R(34)$	28.142	− 7.147	1
$aQ(7,7)$	N_2O $R(32)$	26.820	− 1.105	0.05
$sQ(7,6)$	CO_2 $P(36)$	27.246	4.321	1
$aQ(7,6)$	CO_2 $R(4)$	28.128	− 5.203	1
$aQ(7,3)$	N_2O $R(33)$	19.227	− 1.210	0.15
$aQ(8,8)$	CO_2 $R(2)$	23.530	2.989	0.3
$sQ(8,7)$	N_2O $P(13)$	23.230	− 0.002	0.001
$aQ(8,7)$	N_2O $R(31)$	28.721	− 5.489	1
$sQ(8,6)$	CO_2 $P(34)$	24.346	3.627	1.5
$sQ(9,8)$	N_2O $P(15)$	25.577	1.920	0.5
$aQ(9,8)$	N_2O $R(29)$	20.744	2.913	0.18
$aQ(9,7)$	N_2O $R(30)$	31.052	−10.317	1.5
$sQ(9,6)$	CO_2 $P(32)$	24.389	5.889	2.2
$sQ(9,6)$	N_2O $P(7)$	24.990	6.491	2.2
$aQ(9,6)$	CO_2 $R(2)$	27.213	− 8.714	1
$aQ(10,10)$	N_2O $R(27)$	27.820	0.786	0.05
$sQ(11,9)$	N_2O $P(14)$	21.725	0.654	0.5
$aQ(11,9)$	N_2O $R(26)$	23.114	− 2.043	0.15
Two-photon spectral lines of $^{15}NH_3$				
$sR(1,1)$	CO_2 $R(8)$	27.212	4.587	2.5
$sQ(3,3)$	N_2O $P(14)$	22.024	− 0.765	0.6
$aQ(3,3)$	N_2O $R(29)$	27.656	− 4.867	1
$sQ(4,4)$	N_2O $P(15)$	23.352	0.306	0.3
$sQ(5,4)$	CO_2 $P(38)$	30.288	8.690	2.5
$sQ(5,3)$	CO_2 $P(36)$	23.419	3.147	1.5
$sQ(6,6)$	N_2O $P(18)$	28.012	4.090	2.7
$aQ(6,3)$	N_2O $R(27)$	21.502	− 2.714	0.15
$sQ(7,7)$	N_2O $P(20)$	31.468	6.915	2.8
$aQ(7,7)$	CO_2 $P(2)$	29.940	− 5.387	0.8
$aQ(7,7)$	N_2O $R(25)$	28.558	− 4.005	2.7
$sQ(7,6)$	CO_2 $P(40)$	32.566	10.720	2.6
$sQ(7,6)$	N_2O $P(16)$	28.905	7.059	2.7

[a] CO_2 laser lines are all in the 10.6-μm region, except one with an asterisk, which is in the 9.4-μm region.
[b] Estimated uncertainty for ν_m and $\Delta\nu$ is 0.03 GHz.

the N_2O $R(37)$ line. For this line, $\Delta\nu$ is small ($\Delta\nu=\nu_0-\nu_l=-288.5$ MHz) and the contribution of $\chi^{(7)}$ given in Eq. (30) dominates. As a result the Lamb dip has the Lorentzian absorption shape (note that the picture shows a derivative of the line because of the frequency modulation and phase-sensitive detection). Figure 6(b) shows the two-photon transition $aQ(3,3)$ observed by using the N_2O $R(36)$ line. This line, for which $\Delta\nu=1228.1$ MHz, corresponds to intermediate case, where the line shape is a mixture of absorption and dispersion shape. For such a line the line shape changes when the pressure of the gas and the microwave power are varied according to Eq. (31). Figure 6(c) shows the two-photon transition $aR(5,4)$ observed by using the CO_2 $R(30)$ line in the 9.4-μm region. For this line, $\Delta\nu=-1542.2$ MHz and the contribution of $\chi^{(5)}$ given in Eq. (27) is dominant; the line is of a pure dispersion shape (note again that the signal given in the figure is a derivative of the line). Most of the observed two-photon Lamb dips were of dispersion shape resulting from $\chi^{(5)}$.

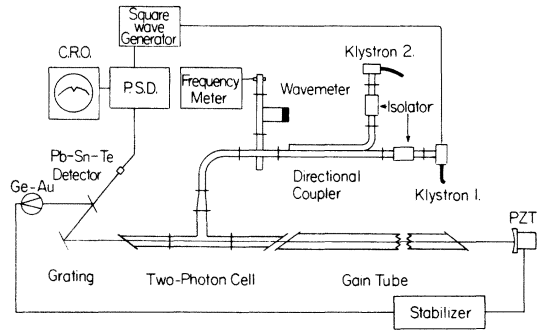

FIG. 5. Block diagram of the apparatus used for the ir-MW two-photon Lamb-dip spectroscopy.

The linewidth of the Lamb dips is typically 0.4 MHz (half width at half-maximum) and is caused by pressure broadening and laser instability. This allowed us to measure the microwave frequency

with an uncertainty of less than 0.1 MHz. However, because of the uncertainty of the laser frequency arising from our method of stabilization, we estimate the accuracy of the infrared spectrum thus measured to be 3 MHz when a CO_2 line is used and 6 MHz when an N_2O line is used. This will be improved if we perform the experiment using a laser stabilized by the method of Freed and Javan.[21]

The observed two-photon Lamb dips are listed in Table II. Altogether, 31 two-photon Lamb dips have been observed for $^{14}NH_3$ and $^{15}NH_3$. This number could have been increased if more powerful klystrons were available. There are several cases where a consistency check can be made in Table II. For example, the $sQ(5, 3)$ two-photon transition has been observed by using both the N_2O $P(7)$ line and the CO_2 $P(32)$ line. The difference of the $\Delta\nu$ values for these two cases, 581.6 MHz, agrees with the frequency difference of the two laser lines, 586.6 MHz, observed by an accurate beating method.[22,23] Another interesting example of internal check is provided by a four-level system involving the infrared transitions $asR(1, 1)$ (ν_R) and $saQ(1, 1)$ (ν_Q), which were measured by two-photon transitions using the CO_2 $R(14)$ line and the N_2O $R(37)$ line, respectively. Because of an accidental near degeneracy of the lower inversion level of the $J=2$, $K=1$ level and the upper inversion level of the $J=1$, $K=1$ level in the ν_2 vibrational state (see Fig. 7), the transition between them (ν) was observed in the millimeter wave region. From the formula $\nu_R=\nu_Q+\nu_m-\nu$, where ν_m is the ground-state inversion frequency, and the two-photon frequency, the frequency of the N_2O $R(37)$ line was determined to be 29 020 129 ± 3 MHz,[24] which differed by 44 MHz from the then-available best N_2O frequency.[25] Subsequent study of the N_2O frequency[23] locates the N_2O $R(37)$ line at 29 020 130.449 MHz, in good agreement with our value.

(a) (b) (c)

FIG. 6. Examples of ir-MW two-photon Lamb dips. (a) The $aQ(1, 1)$ two-photon Lamb dip of NH_3 observed by using the N_2O $R(37)$ line ($\nu_m=23\,983.0$, $\Delta\nu=-288.5$ MHz). (b) The $aQ(3,3)$ two-photon Lamb dip observed by using the N_2O $R(36)$ line ($\nu_m=22\,641.0$, $\Delta\nu=1229.1$ MHz). (c) The $aR(5,4)$ two-photon Lamb dip observed by using the CO_2 $R(30)$ line in the 9.4-μm region ($\nu_m=24\,195.2$, $\Delta\nu=-1542.2$ MHz). The pressure of the sample was 20–40 mTorr and the time constant of detection was 10 msec. Note the variation of line shape depending on $\Delta\nu$.

C. Coherence splitting

For certain cases, such as in the $aR(5,K)$ two-photon transitions with $K=5$, 4 and 3, the Lamb dips appear very close together and we needed some means of assigning the dips unambiguously. The coherence splitting of the Lamb dips was used

TABLE II. Two-photon Lamb-dip lines of $^{14}NH_3$.

Two-photon transition	Laser lines [a]	ν_m [b] (MHz)	$\Delta\nu$ [b] (MHz)
$aQ(1,1)$	N_2O $R(37)$	23 983.0	− 288.5
$sR(1,1)$	CO_2 $R(14)$	22 249.0	−1445.5
$aQ(2,2)$	CO_2 $R(8)$	22 782.4	940.2
$sQ(2,1)$	N_2O $P(8)$	24 699.0	1600.2
$aQ(3,3)$	N_2O $R(36)$	22 641.0	1229.1
$sQ(3,2)$	N_2O $P(8)$	23 173.0	338.9
$aR(5,5)$	CO_2 $R(30)$*	25 609.5	−1076.6
$aQ(5,5)$	CO_2 $R(6)$	27 511.5	−2978.6
$aR(5,4)$	CO_2 $R(30)$*	24 195.2	−1542.2
$sQ(5,4)$	N_2O $P(9)$	21 337.4	−1315.6
$aQ(5,4)$	CO_2 $R(6)$	22 085.0	568.0
$aR(5,3)$	CO_2 $R(30)$*	22 547.0	−1261.7
$sQ(5,3)$	CO_2 $P(32)$	22 245.0	959.7
$sQ(5,3)$	N_2O $P(7)$	22 826.4	1541.3
$sQ(6,5)$	N_2O $P(10)$	21 238.0	−1494.5
$aQ(7,7)$	N_2O $R(32)$	26 827.8	−1112.7
$aQ(7,5)$	CO_2 $R(4)$	20 172.4	632.4
$aQ(8,8)$	CO_2 $R(2)$	23 536.6	2982.3
$sQ(8,7)$	N_2O $P(13)$	23 239.6	7.4
$sQ(8,6)$	CO_2 $P(34)$	24 330.8	3611.6
$sQ(8,5)$	N_2O $P(6)$	19 719.2	910.5
$sQ(9,8)$	N_2O $P(15)$	25 574.8	1917.3
$aQ(9,6)$	N_2O $R(30)$	19 819.6	−1320.3
$aQ(10,10)$	N_2O $R(27)$	27 809.1	795.6
$sQ(11,9)$	N_2O $P(14)$	21 699.6	628.9
$aQ(11,9)$	N_2O $R(26)$	23 114.0	−2043.3
Two-photon Lamb-dip lines of $^{15}NH_3$			
$sR(2,2)$	CO_2 $R(40)$	23 029.0	379.2
$aQ(3,2)$	N_2O $R(29)$	23 877.2	−2093.2
$aQ(3,1)$	N_2O $R(29)$	21 510.2	− 307.9
$sQ(4,4)$	N_2O $P(15)$	23 361.2	315.1
$aQ(4,4)$	N_2O $R(28)$	21 793.0	1253.1
$sQ(5,3)$	CO_2 $P(36)$	23 433.0	3161.0

[a] CO_2 laser lines are all in the 10.6-μm region, except those with an asterisk, which are in the 9.4-μm region.

[b] Estimated uncertainty for ν_m and $\Delta\nu$ is 3 MHz and 6 MHz for lines measured using CO_2 and N_2O laser lines, respectively.

for this purpose. The energy-level scheme and the observed splitting are shown in Fig. 8. In order to observe this splitting we used klystron 2 in Fig. 5 and tuned the second microwave frequency ν'_m into resonance with the inversion transitions. When ν'_m was tuned to resonance, the two-photon Lamb dip was observed to split into a doublet. Since the inversion frequencies of NH_3 are well known,[7] we could assign the dip. The coherence splitting is well-known in microwave spectroscopy[7] and coherence splitting of laser Lamb dips was reported earlier.[3,26,27] The magnitude of the observed splitting is consistent with the matrix element $\langle 1|\vec{\mu}_p \cdot \vec{E}_m|2\rangle/h = \mu_p E_m K M/[J(J+1)]$. Because of the inhomogeneity of the microwave field, the individual M components were not resolved (see Ref. 28 for a case where the M components were resolved in a microwave experiment). The relative positions of the $saR(5,K)$ transitions and observed two-photon Lamb dips are shown in Fig. 9. It is interesting to note that the frequencies of these transitions do not vary uniformly as K changes. This is because of a subtraction of rather large J, K dependence of inversion and rotation energies. Figure 9 also shows the very high resolution of the two-photon Lamb-dip method compared with conventional infrared spectroscopy (the trace at the top of Fig. 9), where these lines are not resolved at all.

D. Double resonance

During the search for two-photon Lamb dips many double-resonance signals were observed.

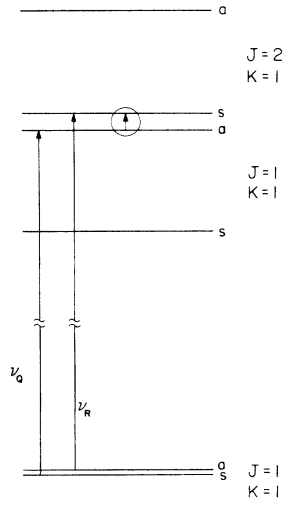

FIG. 7. Inversion-rotation-vibration energy levels of NH_3 showing the $saQ(1,1)$ transition (ν_Q) and the $asR(1,1)$ transition (ν_R). The $J=2 \leftarrow 1$ ($s \leftarrow a$) transition (circled) was measured in the millimeter wave region; therefore ν_Q and ν_R are related accurately.

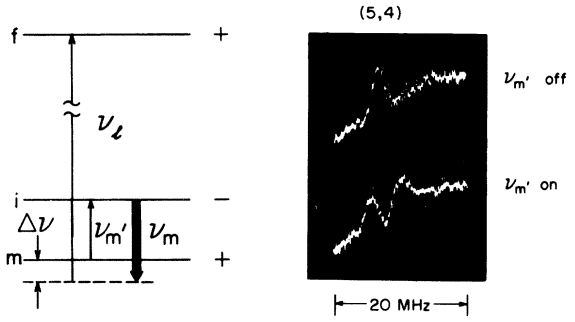

FIG. 8. Energy-level scheme and observed coherence splitting of the $aR(5,4)$ two-photon Lamb dip. The microwave radiation ν'_m causes the splitting of the two-photon ($\nu_l - \nu_m$) Lamb dip.

Their appearance was quite unexpected, since for all laser lines except one [the N_2O $P(13)$ line, which will be discussed below] the laser frequencies are well outside the Doppler profile. The energy-level diagram is given in Fig. 10. Double-resonance signals are caused by a variation of the

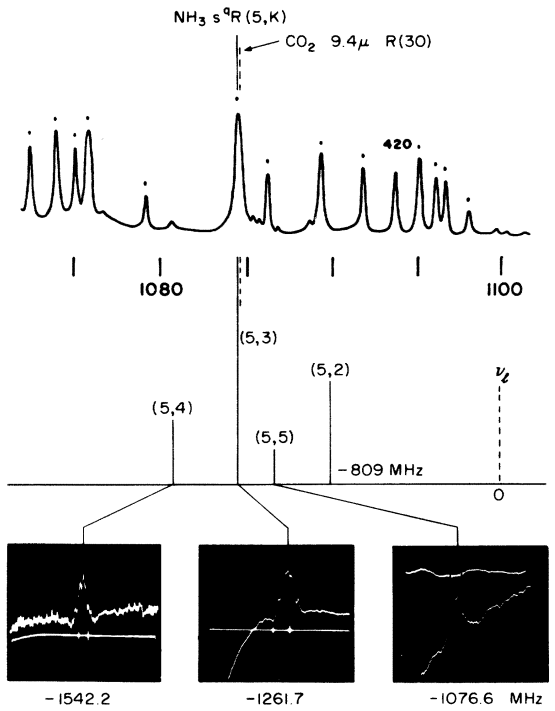

FIG. 9. $saR(5,K)$ transitions of NH_3 with $K=5$, 4, 3, and 2. The top trace shows the spectrum of NH_3 using a conventional infrared spectrometer, where these transitions are not resolved. The bottom pictures show two-photon Lamb dips corresponding to $K=5$, 4, and 3. The middle drawing shows relative positions of the transitions and the laser line. The increase in frequency scale from the top picture to the bottom picture is more than 10^4.

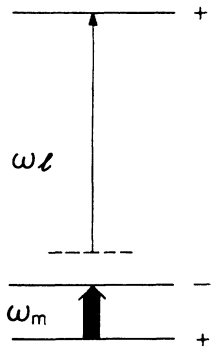

FIG. 10. Energy-level scheme for off-resonance double-resonance experiments. The microwave pumping of molecules at ω_m causes a variation in the dispersion characteristics of the gas for the off-resonant infrared frequency ω_l, which affects the laser power through a frequency shift of the laser.

dispersion as a result of the microwave pumping of molecules. Because of the intracavity arrangement discussed in Sec. II E, this results in the change of laser output power. This interpretation is consistent with the observation that the phase of the double-resonance signal varies depending on whether the laser frequency is set above or below the center of the gain profile. Such an effect has been observed also in other double-resonance experiments,[29] and a semiquantitative theory has been reported in Ref. (9). A more detailed discussion of such double resonance using dispersion characteristics of the gas will be given elsewhere. Figure 11 shows an example of the double-resonance signal corresponding to a $J=5$, $K=3$ inversion doublet. For this double-resonance signal $\Delta\nu = \nu_0 - \nu_l = -1261.7$ MHz. The off-resonant pumping by the laser is negligible and the signal is almost completely due to dispersive effect. It should be remembered that although the absorption is inversely proportional to the square of $\Delta\nu$, the dispersion is inversely proportional to $\Delta\nu$; therefore the dispersion "tail" extends much further than the absorption tail. In fact we could observe almost all of the strong NH_3 inversion transitions by this method in spite of the fact that for some of them the laser frequency was off by more than several wave numbers. This will be very useful for double-resonance experiments without coincidence. It is easy to discriminate between the two-photon Lamb dips and the double-resonance signal because the position of the former moves with the laser frequency tuning, whereas that of the latter does not.

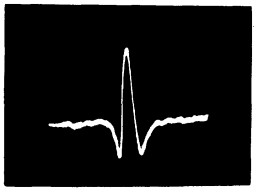

FIG. 11. Example of off-resonance double resonance, corresponding to the (5,3) inversion doublet of NH_3. The laser line used was the CO_2 $R(30)$ line in the 9.4-μm region, which differs from the $saR(5,3)$ vibration-rotation transition by $\Delta\nu = -1261.7$ MHz. The pressure of the gas was 70 mTorr and the time constant of detection was 3 msec.

The N_2O $P(13)$ line and the $aQ(8,7)$ line of NH_3 coincides with the Doppler profile. For such cases we could observe the two-photon Lamb dip and the double-resonance signal within the sweep of the klystron. An example of such a sweep is shown in Fig. 12.

V. DISCUSSION

The results of this paper demonstrate that for molecules with a large dipole moment and favorable energy-level scheme it is possible to conduct systematic infrared spectroscopy in the 10-μm region by using ir-MW two-photon processes. Extension of this method to the 5-μm region by using many lines of the CO laser is feasible. It should be remembered that we have used neither particularly high microwave power nor a microwave-resonant cavity. The use of these will greatly extend the range of two-photon spectroscopy.

The ν_2 vibration-rotation transitions determined in this paper are summarized in Table III, with the hope that they may be useful as frequency standards for laser spectroscopy in the 10-μm region. Shimizu's results[19] of laser Stark spec-

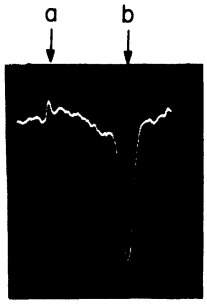

FIG. 12. Special case of coincidence between the N_2O $P(13)$ line and the $asQ(8,7)$ transition of NH_3. The arrow a indicates the ir-MW two-photon Lamb dip and the arrow b indicates double-resonance signal. Their separation here was 7.4 MHz. This can vary owing to the high-frequency Stark effect for high radiation fields. The gas pressure was 0.5 mTorr and the time constant of detection was 10 msec.

TABLE III. Infrared spectrum of the ν_2 band of $^{14}NH_3$.

Infrared transition	ν (cm^{-1})	Method [a]	Infrared transition	ν (cm^{-1})	Method [a]
$asQ(9,8)$	926.045 84	b	$saQ(5,5)$	966.151 00	a
$asQ(11,9)$	926.884 45	b	$saQ(5,4)$	966.269 31	a
$asQ(6,6)$	927.3234	c	$saQ(5,3)$	966.3804	c
$asQ(8,7)$	927.741 96	b	$saQ(5,2)$	966.475	d
$asQ(5,5)$	928.7547	c	$saQ(4,4)$	966.816	d
$asQ(7,6)$	929.1616	c	$saQ(4,3)$	966.908	d
$asQ(4,4)$	929.8984	c	$saQ(3,3)\,\Delta K=3$	967.2502	c
$asQ(9,7)$	929.969	d	$saQ(3,3)$	967.346 32	b
$asQ(6,5)$	930.306 53	b	$saQ(3,2)$	967.4073	c
$asQ(3,3)$	930.7557	c	$saQ(2,2)$	967.738 59	a
$asQ(8,6)$	931.121 90	a	$saQ(2,1)$	967.777	d
$asQ(5,4)$	931.177 35	b	$saQ(1,1)$	967.997 74	b
$asQ(2,2)$	931.3336	c	$asR(1,1)$	971.882 04	a
$asQ(3,2)$	932.094 02	b	$asR(2,2)$	991.6914	c
$asQ(10,7)$	932.233	d			
$asQ(2,1)$	932.136 10	b	$saR(3,3)$	1046.376	d
$asQ(5,3)$	932.992 43	a	$saR(5,4)$	1084.583 71	a
$asQ(4,2)$	933.0762	c	$saR(5,3)$	1084.593 06	a
$asQ(9,6)$	933.1571	c	$saR(5,5)$	1084.599 24	a
$asQ(8,5)$	933.826 00	b	$saR(5,2)$	1084.6082	c
$saQ(11,9)$	960.019 90	b			
$saQ(10,10)$	960.852 32	b	Infrared spectrum of the ν_2 band of $^{15}NH_3$		
$saQ(9,8)$	962.3878	c	$asQ(7,7)$	921.7546	c
$saQ(9,7)$	962.6736	c	$asQ(6,6)$	923.4536	c
$saQ(9,6)$	962.973 68	b	$asQ(7,6)$	925.3320	c
$saQ(8,8)$	963.362 62	a	$asQ(4,4)$	925.992 40	b
$saQ(8,7)$	963.5582	c	$asQ(3,3)$	926.8380	c
$saQ(8,6)$	963.651	d	$asQ(5,4)$	927.2982	c
$saQ(7,7)$	964.424 10	b	$asQ(5,3)$	929.122 88	a
$saQ(7,6)$	964.5954	c	$saQ(7,7)$	959.2126	c
$saQ(7,5)$	964.790 06	a	$saQ(6,3)$	960.7353	c
$saQ(7,4)$	964.982	d	$saQ(4,4)$	961.601 77	b
$saQ(7,3)$	965.1373	c	$saQ(3,3)$	962.1283	c
$saQ(6,6)$	965.355	d	$saQ(3,2)$	962.220 80	b
$saQ(6,5)$	965.501	d	$saQ(3,1)$	962.280 35	b
$saQ(6,4)$	965.6520	c	$asR(1,1)$	967.8602	c
$saQ(6,3)$	965.792	d	$asR(2,2)$	987.632 83	a

[a] Lines marked "a" and "b" were measured by the two-photon Lamb-dip method with CO_2 and N_2O laser lines, respectively. The lines marked "c" were measured by straight two-photon absorption. The lines marked "d" were measured by Shimizu (Ref. 19) by laser Stark spectroscopy. The estimated uncertainties are 0.0001, 0.0002, 0.001, and 0.001 cm^{-1} for a, b, c, and d, respectively.

troscopy are also included in Table III for convenience. The lines marked "a" and "b" were measured with the two-photon Lamb-dip method by using the CO_2 and the N_2O laser, respectively; we estimate the uncertainty of these to be 0.0001 cm^{-1} (3 MHz) and 0.0002 cm^{-1}, respectively. All other lines have an uncertainty of 0.001 cm^{-1}. If we use Freed and Javan's method of laser stabilization,[21] it will be possible to reduce this uncertainty by two orders of magnitude. For such measurements, correction of the high-frequency Stark shift given in Eq. (8) will be necessary. We will then have infrared transition frequencies with the absolute accuracy of microwave spectroscopy. Such accurate measurements may be useful for infrared astronomy in the future.

Although NH_3 is one of the most well-studied molecules, the detailed effect of the nonrigidity of the molecule on the vibration-rotation levels has been studied by few people.[30,31] Thus far,

most analysis has been done by using a semiempirical expansion in the rotational quantum numbers J and K. This is in contrast with the problem of internal rotation (for example, CH_3OH), where detailed theory accounts for the effect of nonrigidity on the vibration-rotation energy levels. In order to analyze the accurately measured spectrum of NH_3 given in this paper some new approach, such as that given in Ref. 31, will be needed.

ACKNOWLEDGMENT

We would like to thank A. E. Douglas for a critical reading of this paper.

---

*Present address: Optical Physics Division, National Bureau of Standards, Washington, D. C. 20234.

[1]See, for example, S. H. Autler and C. H. Townes, Phys. Rev. 100, 703 (1955).
[2]T. Oka and T. Shimizu, Appl. Phys. Lett. 19, 88 (1971).
[3]S. M. Freund and T. Oka, Appl. Phys. Lett. 21, 60 (1972).
[4]S. M. Freund, J. W. C. Johns, A. R. W. McKellar, and T. Oka, J. Chem. Phys. 59, 3445 (1973).
[5]A preliminary report of this work was published by T. Oka, in *Laser Spectroscopy*, edited by R. G. Brewer and A. Mooradian (Plenum, New York, 1974).
[6]M. Göppert-Mayer, Ann. Phys. (Leipz.) 9, 273 (1931).
[7]C. H. Townes and A. L. Schawlow, *Microwave Spectroscopy* (McGraw-Hill, New York, 1955).
[8]T. Oka and T. Shimizu, Phys. Rev. A 2, 587 (1970).
[9]T. Oka, *Les Houches Lectures* (North-Holland, Amsterdam, 1976).
[10]L. D. Landau and E. M. Lifshitz, *Quantum Mechanics, Non-Relativistic Theory* (Fizmatgiz, Moscow, 1963).
[11]T. Shimizu, F. O. Shimizu, R. Turner, and T. Oka, J. Chem. Phys. 55, 2822 (1971).
[12]M. Born, Optik (Springer, Berlin, 1933).
[13]R. Karplus and J. Schwinger, Phys. Rev. 73, 1020 (1948).
[14]R. L. Legan, J. A. Roberts, E. A. Rinehart, and C. C. Lin, J. Chem. Phys. 43, 4337 (1965).
[15]F. Shimizu, Phys. Rev. A 10, 950 (1974).
[16]W. E. Lamb, Jr., Phys. Rev. 134, A1429 (1964).
[17]M. Sargent III, M. O. Scully, and W. E. Lamb, Jr., *Laser Physics* (Addison-Wesley, Reading, Mass., 1974).
[18]S. M. Freund, M. Römheld, and T. Oka, Phys. Rev. Lett. 35, 1497 (1975).
[19]F. Shimizu, J. Chem. Phys. 52, 3572 (1969).
[20]J. S. Garing, H. H. Nielsen, and K. N. Rao, J. Mol. Spectrosc. 3, 496 (1959).
[21]C. Freed and A. Javan, Appl. Phys. Lett. 17, 53 (1970).
[22]F. R. Petersen, D. G. McDonald, J. D. Cupp, and D. L. Danielson, Phys. Rev. Lett. 31, 573 (1973).
[23]G. B. Whitford, K. J. Siemsen, H. D. Riccius, and G. R. Hanes, Opt. Commun. 14, 70 (1975).
[24]F. Y. Chu and S. M. Freund, J. Mol. Spectrosc. 48, 183 (1973).
[25]D. R. Sokoloff and A. Javan, J. Chem. Phys. 56, 4028 (1972).
[26]M. Takami and K. Shimoda, Jpn. J. Appl. Phys. 11, 1648 (1972).
[27]R. F. Curl, Jr., and T. Oka, J. Chem. Phys. 58, 4908 (1973).
[28]T. Oka, Can. J. Phys. 47, 2343 (1969).
[29]W. A. Kreiner and T. Oka, Can. J. Phys. 53, 2000 (1975).
[30]W. T. Week, K. T. Hecht, and D. M. Dennison, J. Mol. Spectrosc. 8, 30 (1962).
[31]D. Papoušek, J. M. R. Stone, and V. Špirko, J. Mol. Spectrosc. 48, 17 (1973).

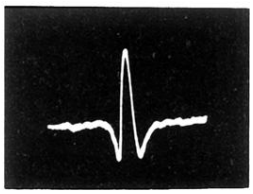

FIG. 11. Example of off-resonance double resonance, corresponding to the (5,3) inversion doublet of NH_3. The laser line used was the CO_2 $R(30)$ line in the 9.4-μm region, which differs from the $saR(5,3)$ vibration-rotation transition by $\Delta\nu = -1261.7$ MHz. The pressure of the gas was 70 mTorr and the time constant of detection was 3 msec.

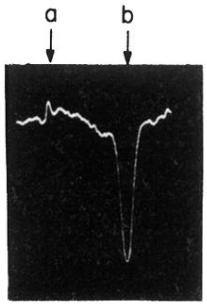

FIG. 12. Special case of coincidence between the N_2O $P(13)$ line and the $asQ(8,7)$ transition of NH_3. The arrow a indicates the ir-MW two-photon Lamb dip and the arrow b indicates double-resonance signal. Their separation here was 7.4 MHz. This can vary owing to the high-frequency Stark effect for high radiation fields. The gas pressure was 0.5 mTorr and the time constant of detection was 10 msec.

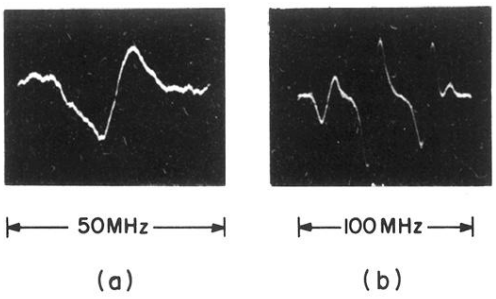

FIG. 4. Examples of ir-MW two-photon absorption signals. (a) The $sQ(4,4)$ two-photon transition of $^{14}NH_3$ observed by using the N_2O $P(11)$ line ($\nu_m = 36.46$, $\Delta\nu = 12.32$ GHz). Sample pressure was 2 Torr and the time constant of detection was 30 msec. (b) The $sQ(4,4)$ two-photon transition of $^{15}NH_3$ observed by using the N_2O $P(15)$ line ($\nu_m = 23358$, $\Delta\nu = 312$ MHz). Sample pressure was 0.3 Torr. The structure of the line is caused by microwave mismatch.

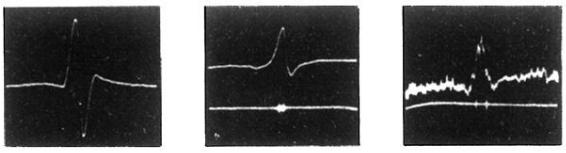

(a) (b) (c)

FIG. 6. Examples of ir-MW two-photon Lamb dips. (a) The $aQ(1,1)$ two-photon Lamb dip of NH_3 observed by using the N_2O $R(37)$ line ($\nu_m = 23\,983.0$, $\Delta\nu = -288.5$ MHz). (b) The $aQ(3,3)$ two-photon Lamb dip observed by using the N_2O $R(36)$ line ($\nu_m = 22\,641.0$, $\Delta\nu = 1229.1$ MHz). (c) The $aR(5,4)$ two-photon Lamb dip observed by using the CO_2 $R(30)$ line in the 9.4-μm region ($\nu_m = 24\,195.2$, $\Delta\nu = -1542.2$ MHz). The pressure of the sample was 20–40 mTorr and the time constant of detection was 10 msec. Note the variation of line shape depending on $\Delta\nu$.

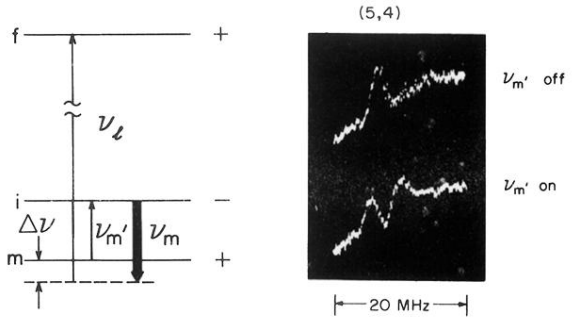

FIG. 8. Energy-level scheme and observed coherence splitting of the $aR(5,4)$ two-photon Lamb dip. The microwave radiation ν'_m causes the splitting of the two-photon $(\nu_l - \nu_m)$ Lamb dip.

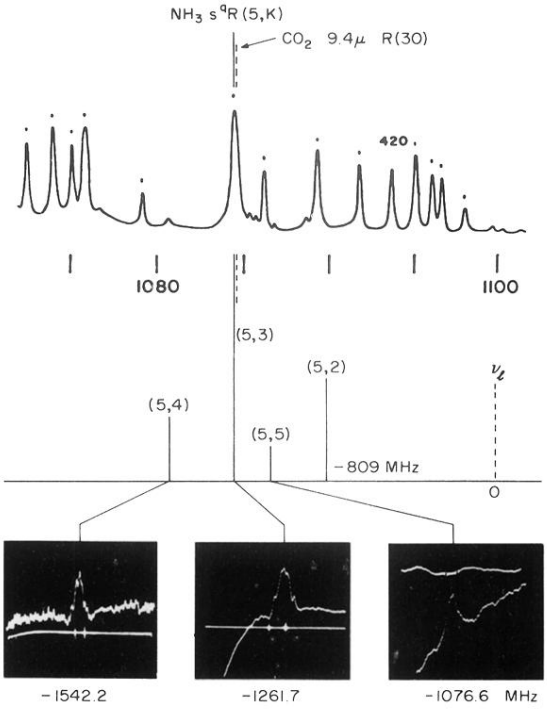

FIG. 9. $saR(5,K)$ transitions of NH_3 with $K=5$, 4, 3, and 2. The top trace shows the spectrum of NH_3 using a conventional infrared spectrometer, where these transitions are not resolved. The bottom pictures show two-photon Lamb dips corresponding to $K=5$, 4, and 3. The middle drawing shows relative positions of the transitions and the laser line. The increase in frequency scale from the top picture to the bottom picture is more than 10^4.